Variable kinematic shell elements for composite laminates accounting for hygrothermal effects

Variable kinematic shell elements for composite laminates accounting for hygro-thermal effects

M. Cinefra, M. Petrolo, G. Li and E. Carrera

MUL^2 Group, Department of Mechanical and Aerospace Engineering,
Politecnico di Torino, Corso Duca degli Abruzzi 24, 10129 Torino, Italy.

Submitted to Journal of Thermal Stresses

Keywords:
finite elements, Carrera Unified Formulation, hygrothermal, trigonometric, exponential, shell.

Author and address for Correspondence
Dr. Maria Cinefra
Associate Professor,
MUL^2 Group, Department of Mechanical and Aerospace Engineering
Politecnico di Torino,
Corso Duca degli Abruzzi, 24,
10129 Torino, ITALY,
tel +39 011 090 6845, fax +39 011 090 6899
e.mail: maria.cinefra@polito.it

Abstract

This paper presents advanced shell models for the steady state hygrothermal analysis of composite laminates. The Carrera Unified Formulation is used to derive refined models that include both Layer-Wise (LW) and Equivalent Single Layer (ESL) models. The governing equations are derived from the Principle of Virtual Displacement (PVD) taking into account thermal and hygroscopic effects. The geometrical relations for the exact cylindrical geometry are here considered. Through-the-thickness variations of temperature and moisture concentration are calculated by solving the Fourier equation and the Fick law, respectively. The Mixed Interpolation of Tensorial Component (MITC) method is applied to a nine-node shell element to contrast the membrane and shear locking phenomena. Simply-supported cross-ply cylindrical shells with anti-symmetrical lamination subjected to bisinusoidal thermal/hygroscopic loads are analyzed considering various thickness/curvature ratios. Results obtained with assumed linear and calculated temperature/hygroscopic profiles are presented. Variable kinematics are compared regarding both accuracy and computational costs. The results show that all the kinematics can approximate the transverse shear stress distribution through the thickness with satisfactory accuracy when sufficient expansion terms are adopted. In some cases, miscellaneous expansions can lead to significant reductions in computational costs. The results here presented can be used as benchmark solutions for future works.

Introduction

The efficient load-carrying capabilities of shell structures make them very useful in a variety of engineering applications. The continuous development of new structural materials leads to ever increasingly complex structural designs that require careful analysis. Moreover, such structures often undergo environmental conditions, e.g. high temperature, and humidity. Hygrothermal effects can lead to the reduction in both constitutive properties and strength of fiber reinforced polymer composites [1, 2]. The possible high hygrothermal residual stress state is a serious issue in the design of laminated composite structures.Efficient mechanical models with the ability to capture the hygrothermal elastic behaviors of multilayered structures are of great significance. Although analytical techniques are very important, the use of numerical methods to solve shell mathematical models of complex structures has become an essential ingredient in the design process. The finite element method has been the fundamental numerical procedure for the analysis of the shells.

Studies on thermal elastic behaviors of composite laminates have been reported by many authors.

Miller [3] studied the thermal elastic response of laminated composite shells with arbitrary temperature distributions through the thickness adopting a classical shell theory, and Dumir [4] elaborated the importance of capturing zig-zag displacement distributions in thermal problems of composite laminates. Several higher-order 2D models have also been developed for thermal elastic analysis, among which the model proposed by Wu and Chen [5] is a significant one. In the above described works, an a priori assumed temperature variation profile through the thickness was adopted. Contributions based on assumed linear or constant temperature profiles can also be found in [6–9].

The thermal conduction in solid media can be described by the Fourier equation, which can be solved by adopting the methodology proposed by Tungikar [10]. Concerning thermal elastic analysis of composite laminates, Carrera [11] exploited the partially coupled thermal elastic governing equations and discussed the influence of through-the-thickness variation of temperature by comparing the thermal mechanical response of laminated anisotropic plates; in particular, assumed profiles and calculated profiles obtained by solving the Fourier conduction equation were used. For thin laminated structures, calculated steady state through-the-thickness temperature profiles can be very close to an assumed linear one, while this is not the case for thick laminates [11, 12].

Following Fourier's work [13], Fick pointed out that the diffusion of moisture in solid media follows the same rule as heat does [14]. Moreover, researchers pointed out that thermal conduction coefficients and humidity diffusivity depend on the temperature [2]. Generally speaking, there is an interaction between thermal environment and moisture diffusion[2], but the temperature approaches equilibrium much faster than moisture concentration [15, 16]. By considering the analogy between thermal conduction and moisture diffusion, Szekeres et al. [17, 18] suggested that the methodology used to solve the Fourier equation [10] can be extended to hygroscopic problems, which has been the basis of many later works.

Benkeddad [19, 20] studied the moisture diffusion process in composite plates by taking only the thickness dimension into consideration, leading to a 1D diffusion problem, and the moisture concentration at a given moment was determined by finite difference method. A similar methodology was adopted for the analysis of transient hygroscopic stresses in unidirectional laminated composite plates with cyclic and asymmetrical environmental conditions by Tounsi et al. [21–24]. Abbas [25] and Boukhoulda [26] introduced the Laplace transform to obtain analytical solutions for transient moisture concentration problems. The moisture diffusion analysis was extended to laminated shells by Jacquemin [27] and cyclic environmental conditions by Jacquemin [27] and Tounsi [21]. Patel [28] and Lo et al. [29] con-

sidered the variation of material properties due to temperature and moisture variation for the static response analysis of multilayered plates. Alsubari [30] analyzed the hygrothermal elastic behavior of laminated composite shells under combined thermal and hygroscopic load, but only assumed linear through-the-thickness profiles were adopted.

The Carrera Unified Formulation (CUF) provides a methodology to develop refined models for the analysis of laminated composite structures, enabling FEM models to have variable kinematics of arbitrary order. Many advanced FEM models have been proposed and applied but not restricted to multifield problems. Carrera [31, 32] proposed advanced shell elements for composite laminates based on CUF using both Equivalent Single Layer (ESL) and Layer-Wise (LW) approaches. Trigonometric trial functions were used in combination with Ritz method in [33]. Thermomechanical analysis of functionally graded shells with CUF and analytical methods was reported in [34].

In authors' previous works [12, 35, 36], CUF was applied to thermoelastic problems of cylindrical and spherical laminated structures, and their static bending responses under both assumed linear and calculated temperature profiles, obtained by solving the Fourier equation, were reported. The Mixed Interpolation of Tensorial Components (MITC) [37–40] method was implemented to alleviate lockings. Such an MITC shell element with a variety of thickness functions have been used to investigate the static response of cross-ply laminated plates and shells [41].

In this paper, considering the analogy between moisture diffusion and thermal conduction, the approach that has been successfully used in solving heat conduction problems [12, 35, 36] is extended to steady state hygroelastic problems. This study mainly focuses on the performance of variable and miscellaneous kinematics of shell elements in the analysis of hygrothermal problems. For simplicity, it is assumed that the thermal conductivity and mass diffusivity do not change with temperature. Both the thermal and hygroscopic problems are restricted to steady state conditions.

Geometrical and constitutive relations of laminated shells

The geometry and reference system are indicated in Fig. 1.

Considering a multilayered structure, the square of an infinitesimal linear segment of the lamina ds_k^2,

the associated infinitesimal area $d\Omega$, and volume dV are given by

$$\begin{cases} ds_k^2 = & H_\alpha^{k\,2}\, d\alpha_k^2 \;+\; H_\beta^{k\,2}\, d\beta_k^2 + H_z^{k\,2}\, dz_k^2 \;, \\ d\Omega_k = & H_\alpha^k H_\beta^k\, d\alpha_k\, d\beta_k \;, \\ dV = & H_\alpha^k\, H_\beta^k\, H_z^k\, d\alpha_k\, d\beta_k\, dz_k \;. \end{cases} \tag{1}$$

where the metric coefficients H_α^k, H_β^k and H_z^k of the k^{th} layer of the multilayered shell are:

$$H_\alpha^k = A^k(1 + z_k/R_\alpha^k), \quad H_\beta^k = B^k(1 + z_k/R_\beta^k), \quad H_z^k = 1 \;. \tag{2}$$

R_α^k and R_β^k are the principal radii of the middle surface of the k^{th} layer, A^k and B^k the coefficients of the first fundamental form of Ω_k. In this paper, the attention has been restricted to shells with constant radii of curvature (cylindrical, spherical, toroidal geometries) for which $A^k = B^k = 1$. For more details about shell formulations, one can refer to [42, 43]. Geometrical relations are

$$\begin{aligned} \boldsymbol{\epsilon}_p^k &= \left\{ \epsilon_{\alpha\alpha}^k, \epsilon_{\beta\beta}^k, \epsilon_{\alpha\beta}^k \right\}^T = (\boldsymbol{D}_p^k + \boldsymbol{A}_p^k)\boldsymbol{u}^k \\ \boldsymbol{\epsilon}_n^k &= \left\{ \epsilon_{\alpha z}^k, \epsilon_{\beta z}^k, \epsilon_{zz}^k \right\}^T = (\boldsymbol{D}_{n\Omega}^k + \boldsymbol{D}_{nz}^k - \boldsymbol{A}_n^k)\boldsymbol{u}^k \end{aligned} \tag{3}$$

The explicit form of the introduced arrays is

$$\boldsymbol{D}_p^k = \begin{bmatrix} \frac{\partial_\alpha}{H_\alpha^k} & 0 & 0 \\ 0 & \frac{\partial_\beta}{H_\beta^k} & 0 \\ \frac{\partial_\beta}{H_\beta^k} & \frac{\partial_\alpha}{H_\alpha^k} & 0 \end{bmatrix}, \quad \boldsymbol{D}_{n\Omega}^k = \begin{bmatrix} 0 & 0 & \frac{\partial_\alpha}{H_\alpha^k} \\ 0 & 0 & \frac{\partial_\beta}{H_\beta^k} \\ 0 & 0 & 0 \end{bmatrix}, \quad \boldsymbol{D}_{nz}^k = \begin{bmatrix} \partial_z & 0 & 0 \\ 0 & \partial_z & 0 \\ 0 & 0 & \partial_z \end{bmatrix}, \tag{4}$$

$$\boldsymbol{A}_p^k = \begin{bmatrix} 0 & 0 & \frac{1}{H_\alpha^k R_\alpha^k} \\ 0 & 0 & \frac{1}{H_\beta^k R_\beta^k} \\ 0 & 0 & 0 \end{bmatrix}, \; \boldsymbol{A}_n^k = \begin{bmatrix} \frac{1}{H_\alpha^k R_\alpha^k} & 0 & 0 \\ 0 & \frac{1}{H_\beta^k R_\beta^k} & 0 \\ 0 & 0 & 0 \end{bmatrix} . \tag{5}$$

Considering the expansion caused by the increase of temperature and moisture absorption, the strain

vector can be expressed as follows:

$$\begin{aligned}\boldsymbol{\epsilon}_p^k &= \left\{\epsilon_{\alpha\alpha}^k, \epsilon_{\beta\beta}^k, \epsilon_{\alpha\beta}^k\right\}^T &&= \boldsymbol{\epsilon}_{pu}^k - \boldsymbol{\epsilon}_{p\theta}^k - \boldsymbol{\epsilon}_{p\eta}^k = \boldsymbol{\epsilon}_{pu}^k - \boldsymbol{\alpha}_p^k\theta^k - \boldsymbol{\beta}_p^k\eta^k \\ \boldsymbol{\epsilon}_n^k &= \left\{\epsilon_{\alpha z}^k, \epsilon_{\beta z}^k, \epsilon_{zz}^k\right\}^T &&= \boldsymbol{\epsilon}_{nu}^k - \boldsymbol{\epsilon}_{n\theta}^k - \boldsymbol{\epsilon}_{n\eta}^k = \boldsymbol{\epsilon}_{nu}^k - \boldsymbol{\alpha}_n^k\theta^k - \boldsymbol{\beta}_n^k\eta^k\end{aligned} \tag{6}$$

where α_{ij} are the thermal expansion coefficients, and β_{ij}^k the moisture expansion coefficients, which in an explicit form are

$$\begin{aligned}\boldsymbol{\alpha}_p^k &= \left\{\alpha_1^k \quad \alpha_2^k \quad 0\right\}^T, \quad \boldsymbol{\alpha}_n^k = \left\{0 \quad 0 \quad \alpha_3^k\right\}^T \\ \boldsymbol{\beta}_p^k &= \left\{\beta_1^k \quad \beta_2^k \quad 0\right\}^T, \quad \boldsymbol{\beta}_n^k = \left\{0 \quad 0 \quad \beta_3^k\right\}^T\end{aligned} \tag{7}$$

θ indicates the increment of temperature, and η the moisture absorption. The stress-strain relations are

$$\begin{aligned}\boldsymbol{\sigma}_p^k &= \left\{\sigma_{\alpha\alpha}^k, \sigma_{\beta\beta}^k, \sigma_{\alpha\beta}^k\right\}^T = \boldsymbol{\sigma}_{pu}^k - \boldsymbol{\sigma}_{p\theta}^k - \boldsymbol{\sigma}_{p\eta}^k = \boldsymbol{C}_{pp}^k\boldsymbol{\epsilon}_{pu}^k + \boldsymbol{C}_{pn}^k\boldsymbol{\epsilon}_{nu}^k - \boldsymbol{\lambda}_p^k\theta^k - \boldsymbol{\mu}_p^k\eta^k \\ \boldsymbol{\sigma}_n^k &= \left\{\sigma_{\alpha z}^k, \sigma_{\beta z}^k, \sigma_{zz}^k\right\}^T = \boldsymbol{\sigma}_{nu}^k - \boldsymbol{\sigma}_{n\theta}^k - \boldsymbol{\sigma}_{n\eta}^k = \boldsymbol{C}_{np}^k\boldsymbol{\epsilon}_{pu}^k + \boldsymbol{C}_{nn}^k\boldsymbol{\epsilon}_{nu}^k - \boldsymbol{\lambda}_n^k\theta^k - \boldsymbol{\mu}_n^k\eta^k\end{aligned} \tag{8}$$

where

$$\begin{aligned}\boldsymbol{C}_{pp}^k &= \begin{bmatrix} C_{11}^k & C_{12}^k & C_{16}^k \\ C_{12}^k & C_{22}^k & C_{26}^k \\ C_{16}^k & C_{26}^k & C_{66}^k \end{bmatrix} \qquad \boldsymbol{C}_{pn}^k = \begin{bmatrix} 0 & 0 & C_{13}^k \\ 0 & 0 & C_{23}^k \\ 0 & 0 & C_{36}^k \end{bmatrix} \\ \boldsymbol{C}_{np}^k &= \begin{bmatrix} 0 & 0 & 0 \\ 0 & 0 & 0 \\ C_{13}^k & C_{23}^k & C_{36}^k \end{bmatrix} \qquad \boldsymbol{C}_{nn}^k = \begin{bmatrix} C_{55}^k & C_{45}^k & 0 \\ C_{45}^k & C_{44}^k & 0 \\ 0 & 0 & C_{33}^k \end{bmatrix}\end{aligned} \tag{9}$$

λ_{ij} are the coefficients of thermomechanical coupling and μ_{ij}^k are the coefficients of hygromechanical coupling,

$$\begin{cases} \boldsymbol{\lambda}_p^k = \boldsymbol{C}_{pp}^k\boldsymbol{\alpha}_p^k + \boldsymbol{C}_{pn}^k\boldsymbol{\alpha}_n^k \\ \boldsymbol{\lambda}_n^k = \boldsymbol{C}_{np}^k\boldsymbol{\alpha}_p^k + \boldsymbol{C}_{nn}^k\boldsymbol{\alpha}_n^k \end{cases} \tag{10}$$

$$\begin{cases} \boldsymbol{\mu}_p^k = \boldsymbol{C}_{pp}^k\boldsymbol{\beta}_p^k + \boldsymbol{C}_{pn}^k\boldsymbol{\beta}_n^k \\ \boldsymbol{\mu}_n^k = \boldsymbol{C}_{np}^k\boldsymbol{\beta}_p^k + \boldsymbol{C}_{nn}^k\boldsymbol{\beta}_n^k \end{cases} \tag{11}$$

where $\boldsymbol{\lambda}_p^k$ and $\boldsymbol{\lambda}_n^k$ are the vectors of thermomechanical coupling coefficients, and $\boldsymbol{\mu}_p^k$ and $\boldsymbol{\mu}_n^k$ vectors of hygromechanical coupling coefficients, whose explicit expressions are:

$$\boldsymbol{\lambda}_p^k = \begin{Bmatrix} \lambda_1^k & \lambda_2^k & \lambda_6^k \end{Bmatrix}^T, \quad \boldsymbol{\lambda}_n^k = \begin{Bmatrix} 0 & 0 & \lambda_3^k \end{Bmatrix}^T \tag{12}$$

$$\boldsymbol{\mu}_p^k = \begin{Bmatrix} \mu_1^k & \mu_2^k & \mu_6^k \end{Bmatrix}^T, \quad \boldsymbol{\mu}_n^k = \begin{Bmatrix} 0 & 0 & \mu_3^k \end{Bmatrix}^T \tag{13}$$

The material coefficients C_{ij} depend on the Young, shear, and Poisson moduli, see Reddy's book [44].

Carrera Unified Formulation

According to the CUF, the displacement vector $\boldsymbol{u} = \{u, v, w\}$ in the curvilinear reference system can be expressed utilizing expansion functions as follows:

$$\begin{cases} u(\alpha,\beta,z) = F_0(z)u_0(\alpha,\beta) & +F_1(z)u_1(\alpha,\beta) & +\cdots+F_N(z)u_N(\alpha,\beta) \\ v(\alpha,\beta,z) = F_0(z)v_0(\alpha,\beta) & +F_1(z)v_1(\alpha,\beta) & +\cdots+F_N(z)v_N(\alpha,\beta) \\ w(\alpha,\beta,z) = F_0(z)w_0(\alpha,\beta) & +F_1(z)w_1(\alpha,\beta) & +\cdots+F_N(z)w_N(\alpha,\beta) \end{cases} \tag{14}$$

In a more compact form, when applied to ESL models, CUF can be expressed as:

$$\delta\boldsymbol{u}(\alpha,\beta,z) = F_\tau(z)\delta\boldsymbol{u}_\tau(\alpha,\beta); \qquad \boldsymbol{u}(\alpha,\beta,z) = F_s(z)\boldsymbol{u}_s(\alpha,\beta) \qquad \tau,s = 0,1,...,N \tag{15}$$

Or alternatively in the form of a LW model:

$$\delta\boldsymbol{u}^k(\alpha,\beta,\zeta_k) = F_\tau(\zeta_k)\delta\boldsymbol{u}_\tau^k(\alpha,\beta); \qquad \boldsymbol{u}^k(\alpha,\beta,\zeta_k) = F_s(\zeta_k)\boldsymbol{u}_s^k(\alpha,\beta) \qquad \tau,s = 0,1,...,N \tag{16}$$

where (α,β,z) is the curvilinear reference system (see Fig. 1), and the curvature radii R_α and R_β are constant over the in-plane domain Ω. $\delta\boldsymbol{u}$ indicates the virtual displacement associated with the virtual work, and k is the index of a layer in the laminated shell. $F_\tau^{(k)}$ and $F_s^{(k)}$ are the so called thickness functions whose independent variable is either z defined in the whole thickness domain $z \in [-\frac{h}{2}, \frac{h}{2}]$ for

ESL models, or ζ_k defined in each layer domain $\zeta_k \in [-1, 1]$ for LW models. Depending on the type of expansion functions, N may represent the order of the expansion or the number of expansion terms. $\boldsymbol{u}_s$ represents the unknown primary variables which are the coefficients of corresponding expansion terms, whose independent variables are α and β. τ and s are the index of the expansion terms, and the Einstein summation rule is used.

Higher-Order Theories

In the case of Equivalent Single Layer (ESL) models, Taylor series expansions can be employed as thickness functions:

$$\boldsymbol{u} = F_0\, \boldsymbol{u}_0 \;+\; F_1\, \boldsymbol{u}_1 \;+\; \ldots \;+\; F_N\, \boldsymbol{u}_N \;=\; F_s\, \boldsymbol{u}_s, \qquad s = 0, 1, \ldots, N \tag{17}$$

$$F_0 = z^0 = 1, \quad F_1 = z^1 = z, \quad \ldots, \quad F_N = z^N \tag{18}$$

Classical models, such as those based on the First-Order Shear Deformation Theory (FSDT) [45], can be obtained with an ESL approach with $N = 1$, by imposing a constant transverse displacement through the thickness via penalty techniques. Also, a model based on the hypotheses of Classical Lamination Theory (CLT) [46, 47] can be expressed employing CUF by applying a penalty technique to the constitutive equations to impose null transverse shear strains.

Refined ESL models based on trigonometric and exponential series

In the framework of ESL models, if trigonometric sine series with a constant term are adopted, the displacement vector can be written as follows:

$$\boldsymbol{u}(\alpha, \beta, z) = \boldsymbol{u}_0(\alpha, \beta) + \sin\left(\frac{\pi z}{h}\right) \boldsymbol{u}_1(\alpha, \beta) + ... + \sin\left(\frac{n\pi z}{h}\right) \boldsymbol{u}_N(\alpha, \beta) \tag{19}$$

where h is the thickness of the whole laminated structure and n is the half waves number. If the linear Taylor term is considered, the displacement vector is

$$\boldsymbol{u}(\alpha, \beta, z) = \boldsymbol{u}_0(\alpha, \beta) + z\, \boldsymbol{u}_1(\alpha, \beta) + \sin\left(\frac{\pi z}{h}\right) \boldsymbol{u}_2(\alpha, \beta) + ... + \sin\left(\frac{n\pi z}{h}\right) \boldsymbol{u}_{N+1}(\alpha, \beta) \tag{20}$$

For trigonometric cosine series,

$$\boldsymbol{u}(\alpha,\beta,z) = \boldsymbol{u}_0(x,y) + \cos\left(\frac{\pi z}{h}\right)\,\boldsymbol{u}_1(\alpha,\beta) + ... + \cos\left(\frac{n\pi z}{h}\right)\,\boldsymbol{u}_N(\alpha,\beta) \tag{21}$$

and with the linear term,

$$\boldsymbol{u}(x,y,z) = \boldsymbol{u}_0(\alpha,\beta) + z\,\boldsymbol{u}_1(\alpha,\beta) + \cos\left(\frac{\pi z}{h}\right)\,\boldsymbol{u}_2(\alpha,\beta) + ... + \cos\left(\frac{n\pi z}{h}\right)\,\boldsymbol{u}_{N+1}(\alpha,\beta) \tag{22}$$

Considering the complete trigonometric series,

$$\begin{aligned}\boldsymbol{u}(\alpha,\beta,z) = \boldsymbol{u}_0(\alpha,\beta) + \sin\left(\frac{\pi z}{h}\right)\,\boldsymbol{u}_1(\alpha,\beta) + \cos\left(\frac{\pi z}{h}\right)\,\boldsymbol{u}_2(\alpha,\beta) + ... + \sin\left(\frac{n\pi z}{h}\right)\,\boldsymbol{u}_{2N-1}(\alpha,\beta) + \\ + \cos\left(\frac{n\pi z}{h}\right)\,\boldsymbol{u}_{2N}(\alpha,\beta)\end{aligned} \tag{23}$$

If the linear contribution is considered,

$$\begin{aligned}\boldsymbol{u}(\alpha,\beta,z) = \boldsymbol{u}_0(\alpha,\beta) + z\,\boldsymbol{u}_1(\alpha,\beta) + \sin\left(\frac{\pi z}{h}\right)\,\boldsymbol{u}_2(\alpha,\beta) + \cos\left(\frac{\pi z}{h}\right)\,\boldsymbol{u}_3(\alpha,\beta) + ...+ \\ + \sin\left(\frac{n\pi z}{h}\right)\,\boldsymbol{u}_{2N}(\alpha,\beta) + \cos\left(\frac{n\pi z}{h}\right)\,\boldsymbol{u}_{2N+1}(\alpha,\beta)\end{aligned} \tag{24}$$

If exponential series are employed, the displacement field can be expressed as

$$\boldsymbol{u}(\alpha,\beta,z) = \boldsymbol{u}_0(\alpha,\beta) + e^{\frac{z}{h}}\,\boldsymbol{u}_1(\alpha,\beta) + ... + e^{\frac{nz}{h}}\,\boldsymbol{u}_N(\alpha,\beta) \tag{25}$$

and adding the linear term one obtains

$$\boldsymbol{u}(\alpha,\beta,z) = \boldsymbol{u}_0(\alpha,\beta) + z\,\boldsymbol{u}_1(\alpha,\beta) + e^{\frac{z}{h}}\,\boldsymbol{u}_2(\alpha,\beta) + ... + e^{\frac{nz}{h}}\,\boldsymbol{u}_{N+1}(\alpha,\beta) \tag{26}$$

Refined ESL models with Murakami zig-zag function

According to Murakami [48], a zig-zag term can be introduced into Eq. (17) leading to refined ESL zig-zag models,

$$\boldsymbol{u} = \; F_0\,\boldsymbol{u}_0 \; + \; \ldots \; + \; F_N\,\boldsymbol{u}_N \; + \; (-1)^k \zeta_k \boldsymbol{u}_Z. \tag{27}$$

Subscript Z refers to the Murakami zig-zag function. Refined zig-zag models can be obtained by adding the zig-zag term to the Taylor polynomials, trigonometric or exponential series expansions.

Refined LW models based on Legendre polynomials

If Legendre polynomials are adopted, the displacement field defined for a layer k can be expressed as

$$\boldsymbol{u}^k = F_t\, \boldsymbol{u}_t^k + F_b\, \boldsymbol{u}_b^k + F_r\, \boldsymbol{u}_r^k = F_s\, \boldsymbol{u}_s^k, \qquad s = t, b, r\ , \quad r = 2, ..., N. \tag{28}$$

The expansion terms are

$$F_t = \frac{P_0 + P_1}{2}, \quad F_b = \frac{P_0 - P_1}{2}, \quad F_r = P_r - P_{r-2}. \tag{29}$$

P_j is the j^{th}-order Legendre polynomial defined in the ζ_k-domain: $-1 \leq \zeta_k \leq 1$. The displacements on the top (t) and bottom (b) surfaces are used as unknown variables and one can impose the following compatibility conditions at the interfaces:

$$u_t^k = u_b^{k+1}, \qquad k = 1, N_l - 1. \tag{30}$$

The employment of hierarchical Legendre polynomials as basis functions for the development of variable kinematic models was presented by Szab, Dster, and Rank [49]. Other implementations of Legendre polynomials in the framework of CUF can be found in [50–52].

Refined LW models adopting Sampling Surfaces method (SaS)

Kulikov [53–55] proposed the Sampling Surfaces method (SaS) as an LW model based on Lagrange interpolation polynomials. Within each layer, an arbitrary number of sampling surfaces parallel to the middle surface are introduced. Each SaS is located at a Lagrange interpolation point, and the displacements at these points are taken as primary unknowns. The present work implements the SaS technique for the MITC9 shell element based on CUF. In SaS, the displacement field can be defined as

$$\boldsymbol{u}^k = F_0\, \boldsymbol{u}_0^k + F_1\, \boldsymbol{u}_1^k + \ldots + F_N\, \boldsymbol{u}_N^k = F_s\, \boldsymbol{u}_s^k, \qquad s = 0, 1, \ldots, N. \tag{31}$$

$F_s(\zeta_k)$ (thickness functions) is a Lagrange polynomial of order N,

$$F_s(\zeta_k) = \prod_{i=0, i\neq s}^{N} \frac{\zeta_k - \zeta_{k_i}}{\zeta_{k_s} - \zeta_{k_i}} \tag{32}$$

ζ_{k_s} are located at the prescribed interpolation points. $\zeta_{k_0} = -1$ and $\zeta_{k_N} = 1$ correspond to the top and bottom positions of the k^{th} layer, respectively.

Through-the-thickness variation of temperature and moisture concentration

The temperature variation through the thickness can be obtained by solving Fourier heat conduction equation as described in [12]. If the temperature on the top and bottom surfaces are given, a priori assumed linear temperature variation profile through-the -thickness can be obtained as follows:

$$\theta(z) = \theta_b + \frac{\theta_t - \theta_b}{h} \cdot (z + \frac{h}{2}) \quad z \in [-\frac{h}{2}, \frac{h}{2}] \tag{33}$$

where the subscripts b and t refer to the bottom and top surfaces, respectively. It is evident that the temperature continuity between two layers can be naturally guaranteed in this manner. Similarly, an assumed linear moisture concentration profile could be described as:

$$\eta(z) = \eta_b + \frac{\eta_t - \eta_b}{h} \cdot (z + \frac{h}{2}) \quad z \in [-\frac{h}{2}, \frac{h}{2}] \tag{34}$$

Alternatively, a more physically meaningful profile can be obtained by solving Fourier heat conduction equation for temperature variation, or the Fick law for moisture concentration distribution. In multi-layered plate and shell structures, for the k^{th} homogeneous orthotropic layer, the Fourier differential equation for heat conduction problems reads:

$$\frac{K_1^k}{(H_\alpha^k)^2}\frac{\delta^2\theta}{\delta\alpha^2} + \frac{K_2^k}{(H_\beta^k)^2}\frac{\delta^2\theta}{\delta\beta^2} + K_3^k\frac{\delta^2\theta}{\delta z^2} = 0 \tag{35}$$

where K_1^k, K_2^k and K_3^k are the thermal conduction coefficients in material coordinates (1,2,3) for the k^{th} layer and will be rotated to the general curvilinear reference system (α, β, z). In the k^{th} layer, K_1^k, K_2^k and K_3^k are assumed to be constants. The relationship between the temperature θ and the transverse

normal heat flux q_z is described by

$$q_z^k = K_3^k \frac{\partial \theta}{\partial z} \tag{36}$$

For multilayered structures, continuity conditions of θ and q_z holds in the thickness direction at each layer interface, reading:

$$\theta_t^k = \theta_b^{k+1}, \quad q_{zt}^k = q_{zb}^{k+1} \qquad k = 1, \cdots, N_l - 1 \tag{37}$$

where N_l is the number of layers in the composite laminate. In this work, the governing equation and boundary conditions are satisfied in each layer by assuming the following temperature field:

$$\theta(\alpha, \beta, z) = \theta_A(z) \cdot \theta_\Omega(\alpha, \beta) \tag{38}$$

where for the cases studied in this paper, θ_Ω is in a bisinusoidal form as follows:

$$\theta_\Omega(\alpha, \beta) = \sin(\frac{m\pi\alpha}{a}) \cdot \sin(\frac{n\pi\beta}{b}) \tag{39}$$

For the solution of the Fourier heat conduction equation, the reader can refer to the authors' previous works [12, 31, 56]. Calculated moisture concentration profiles can be acquired by solving the Fick law, which postulates that the flux J goes from regions of high concentration to areas of low concentration, with a diffusion rate that is proportional to the concentration gradients (spatial derivatives). For a steady state shell structure, the Fick second law can be expressed as

$$\frac{D_1^k}{(H_\alpha^k)^2} \frac{\delta^2 \eta}{\delta \alpha^2} + \frac{D_2^k}{(H_\beta^k)^2} \frac{\delta^2 \eta}{\delta \beta^2} + D_3^k \frac{\delta^2 \eta}{\delta z^2} = 0 \tag{40}$$

where D_1, D_2 and D_3 are the diffusion coefficients (diffusivity), η the moisture concentration. Accordingly, moisture concentration η and diffusion flux through the thickness J_z can be related by

$$J_z^k = D_3^k \frac{\partial \eta}{\partial z} \tag{41}$$

and the continuity of η and J_z at layer interfaces can be imposed as

$$\eta_t^k = \eta_b^{k+1}, \quad J_{zt}^k = J_{zb}^{k+1} \qquad k = 1, \cdots, N_l - 1 \tag{42}$$

Similarly, the 3D hygroscopic field can be described as

$$\eta(\alpha, \beta, z) = \eta_A(z) \cdot \eta_\Omega(\alpha, \beta) \tag{43}$$

If a bisinusoidal load is imposed,

$$\eta_\Omega(\alpha, \beta) = \sin(\frac{m\pi\alpha}{a}) \cdot \sin(\frac{n\pi\beta}{b}) \tag{44}$$

As discussed above, the Fick law can be solved in analogy with the Fourier heat conduction equation under given hygroscopic boundary conditions on the top and bottom surfaces of the laminated structures.

MITC9 shell element and governing equations

This section presents the derivation of the finite element stiffness matrix based on the Principle of Virtual Displacement (PVD) in the case of multilayered doubly curved shells under hygrothermal environmental load. A nine-node shell element adopting the Mixed Interpolation of Tensorial Component (MITC) method is formulated in the framework of CUF. The displacement vector interpolated on the element nodes utilizing Lagrangian shape functions N_i reads

$$\delta \boldsymbol{u}_\tau = N_i \delta \boldsymbol{U}_{\tau_i}, \qquad \boldsymbol{u}_s = N_j \boldsymbol{U}_{s_j} \qquad i, j = 1, \cdots, 9 \tag{45}$$

$\boldsymbol{U}_{s_j}$ and $\delta \boldsymbol{U}_{\tau_i}$ are the nodal displacement vector and its virtual variation, respectively. Therefore, the strain expression (Eq. (6)) becomes

$$\begin{cases} \boldsymbol{\epsilon}_p = F_s(\boldsymbol{D}_p + \boldsymbol{A}_p) N_j \boldsymbol{U}_{s_j} \\ \boldsymbol{\epsilon}_n = F_s(\boldsymbol{D}_{n\Omega} - \boldsymbol{A}_n) N_j \boldsymbol{U}_{s_j} + F_{s,_z} N_j \boldsymbol{U}_{s_j} \end{cases} \tag{46}$$

To contrast the membrane and shear locking of thin shells, a specific interpolation strategy according to MITC method is used to derive the strain components on the nine-node shell element, and the corresponding interpolation points (*tying points*) are illustrated in previous authors' works related to the use of the MITC9 element based on the CUF [57–60].

Considering the constitutive equations (Eq. (8)) and the strain vectors (Eq. (46)), scalar temperature

field θ as well as moisture concentration field η, by applying PVD, one obtains the expression of the internal work for partially coupled hygrothermal problems:

$$\begin{aligned}\delta L_{int} &= \int_{\Omega_k}\int_{A_k} \delta{\boldsymbol{\epsilon}^k}^T \boldsymbol{\sigma}^k H^k_\alpha H^k_\beta d\Omega_k dz = \int_{\Omega_k}\int_{A_k} [\delta{\boldsymbol{\epsilon}_p^k}^T(\boldsymbol{\sigma}^k_{pu} - \boldsymbol{\sigma}^k_{p\theta} - \boldsymbol{\sigma}^k_{p\eta}) + \delta{\boldsymbol{\epsilon}_n^k}^T(\boldsymbol{\sigma}^k_{nu} - \boldsymbol{\sigma}^k_{n\theta} - \boldsymbol{\sigma}^k_{n\eta})] H^k_\alpha H^k_\beta d\Omega_k dz \\ &= \delta L_{ext}\end{aligned} \tag{47}$$

where Ω_k is the in-plane domain of an element and A_k is the thickness domain of layer k of the shell, respectively. δL_{int} represents the variation of the internal work, while δL_{ext} is the external work. Noting that in this work no mechanical loads are considered, which means that $\delta L_{ext} = 0$, and the internal work δL_{int} is caused purely by the mechanical expansion related to temperature rise and moisture absorption, thus the following expression can be obtained:

$$\begin{aligned}&\int_{\Omega_k}\int_{A_k} (\delta{\boldsymbol{\epsilon}_p^k}^T \boldsymbol{\sigma}^k_{pu} + \delta{\boldsymbol{\epsilon}_n^k}^T \boldsymbol{\sigma}^k_{nu}) H^k_\alpha H^k_\beta d\Omega_k dz \\ &= \int_{\Omega_k}\int_{A_k} (\delta{\boldsymbol{\epsilon}_p^k}^T \boldsymbol{\sigma}^k_{p\theta} + \delta{\boldsymbol{\epsilon}_n^k}^T \boldsymbol{\sigma}^k_{n\theta}) H^k_\alpha H^k_\beta d\Omega_k dz + \int_{\Omega_k}\int_{A_k} (\delta{\boldsymbol{\epsilon}_p^k}^T \boldsymbol{\sigma}^k_{p\eta} + \delta{\boldsymbol{\epsilon}_n^k}^T \boldsymbol{\sigma}^k_{n\eta}) H^k_\alpha H^k_\beta d\Omega_k dz\end{aligned} \tag{48}$$

By substituting the constitutive equations (Eq. (8)), the geometrical relations (Eq. (46)) after the application of MITC method, the displacement expression (Eqs. (15) and (16)), and the FEM discretization (Eq. (45)), the following governing equation can be obtained:

$$\delta \boldsymbol{U}^k_{\tau_i} : \quad \boldsymbol{K}^{k,uu}_{\tau sij} \boldsymbol{U}^k_{s_j} = \boldsymbol{\Theta}^k_{\tau_i} + \boldsymbol{H}^k_{\tau_i} \tag{49}$$

The 3×3 matrix $\boldsymbol{K}^{k,uu}_{\tau sij}$ is the fundamental mechanical nucleus, which is the core unit of the element stiffness matrix according to CUF, and its explicit expression is given in [56]. The stiffness matrix corresponding to each layer within each element can be obtained by applying the Einstein summation rule, then assembled on the laminate level in the framework of either ESL or LW model to build the nodal, and then element stiffness matrix. $\boldsymbol{\Theta}^k_{\tau_i}$ and $\boldsymbol{H}^k_{\tau_i}$ are the equivalent thermal and hygroscopic load

vectors, and their explicit expressions are given in Eq. (50) and Eq. (51), respectively:

$$\boldsymbol{\Theta}^k_{\tau_i} = \left\{ \begin{array}{c} \Theta^{k\tau i}_{\alpha} \\ \Theta^{k\tau i}_{\beta} \\ \Theta^{k\tau i}_{z} \end{array} \right\} = \left\{ \begin{array}{l} \lambda^k_6 J^{\theta k\tau}_{\alpha} W^{\theta k}_{i,\beta} + \lambda^k_1 J^{\theta k\tau}_{\beta} W^{\theta k}_{i,\alpha} \\ \lambda^k_2 J^{\theta k\tau}_{\alpha} W^{\theta k}_{i,\beta} + \lambda^k_6 J^{\theta k\tau}_{\beta} W^{\theta k}_{i,\alpha} \\ \lambda^k_3 J^{\theta k\tau,z}_{\alpha\beta} W^{\theta k}_{i} + \dfrac{\lambda^k_1}{R^k_{\alpha}} J^{\theta k\tau}_{\beta} W^{\theta k}_{i} + \dfrac{\lambda^k_2}{R^k_{\beta}} J^{\theta k\tau}_{\alpha} W^{\theta k}_{i} \end{array} \right\} \tag{50}$$

$$\boldsymbol{H}^k_{\tau_i} = \left\{ \begin{array}{c} H^{k\tau i}_{\alpha} \\ H^{k\tau i}_{\beta} \\ H^{k\tau i}_{z} \end{array} \right\} = \left\{ \begin{array}{l} \mu^k_6 J^{\eta k\tau}_{\alpha} W^{\eta k}_{i,\beta} + \mu^k_1 J^{\eta k\tau}_{\beta} W^{\eta k}_{i,\alpha} \\ \mu^k_2 J^{\eta k\tau}_{\alpha} W^{\eta k}_{i,\beta} + \mu^k_1 J^{\eta k\tau}_{\beta} W^{\eta k}_{i,\alpha} \\ \mu^k_3 J^{\eta k\tau,z}_{\alpha\beta} W^{\eta k}_{i} + \dfrac{\mu^k_1}{R^k_{\alpha}} J^{\eta k\tau}_{\beta} W^{\eta k}_{i} + \dfrac{\mu^k_2}{R^k_{\beta}} J^{\eta k\tau}_{\alpha} W^{k}_{i} \end{array} \right\} \tag{51}$$

$J^{k\tau}_{\alpha}, J^{k\tau}_{\beta}$ and $J^{k\tau,z}_{\alpha\beta}$ are the integrals in the in-plane domain Ω_k of the k^{th} layer. $W^k_i, W^k_{i,\alpha}, W^k_{i,\beta}$ are the integrals defined within the through-the-thickness domain A_k of the same layer,

$$W^{\theta k}_{i} = \int_{\Omega_k} N_i \theta_{\Omega} d\alpha_k d\beta_k, \quad W^{\theta k}_{i,\alpha} = \int_{\Omega_k} \frac{\partial N_i}{\partial \alpha} \theta_{\Omega} d\alpha_k d\beta_k, \quad W^{\theta k}_{i,\beta} = \int_{\Omega_k} \frac{\partial N_i}{\partial \beta} \theta_{\Omega} d\alpha_k d\beta_k \tag{52}$$

$$J^{\theta k\tau}_{\alpha} = \int_{A_k} F_{\tau} \theta_k H^k_{\alpha} dz, \quad J^{\theta k\tau}_{\beta} = \int_{A_k} F_{\tau} \theta_k H^k_{\beta} dz, \quad J^{\theta k\tau,z}_{\alpha,\beta} = \int_{A_k} \frac{\partial F_{\tau}}{\partial z} \theta_k H^k_{\alpha} H^k_{\beta} dz \tag{53}$$

$$W^{\eta k}_{i} = \int_{\Omega_k} N_i \eta_{\Omega} d\alpha_k d\beta_k, \quad W^{\eta k}_{i,\alpha} = \int_{\Omega_k} \frac{\partial N_i}{\partial \alpha} \eta_{\Omega} d\alpha_k d\beta_k, \quad W^{\eta k}_{i,\beta} = \int_{\Omega_k} \frac{\partial N_i}{\partial \beta} \eta_{\Omega} d\alpha_k d\beta_k \tag{54}$$

$$J^{\eta k\tau}_{\alpha} = \int_{A_k} F_{\tau} \eta_k H^k_{\alpha} dz, \quad J^{\eta k\tau}_{\beta} = \int_{A_k} F_{\tau} \eta_k H^k_{\beta} dz, \quad J^{\eta k\tau,z}_{\alpha,\beta} = \int_{A_k} \frac{\partial F_{\tau}}{\partial z} \eta_k H^k_{\alpha} H^k_{\beta} dz \tag{55}$$

θ and η denote thermal and hygroscopic cases, respectively. F_{τ} refers to a general expansion term in the displacement field according to CUF, and N_i represents the shape function corresponding to node i in the finite element. For more details, the reader can refer to [12, 31, 56].

Results

The numerical analysis of this work focuses on investigating the capability of a variety of models with variable kinematics in the analysis of laminated structures under hygrothermal environmental loads. This section consists of two numerical cases:

- A two-layer (0°/90°) cylindrical shell under thermal load;
- A two-layer (0°/90°) cylindrical shell under hygroscopic load.

Acronyms are used to indicate the various models used. For ESL, Table 1 shows all the cases used in this paper.

For example, "ES2C2" and "ET1Exp2Z" refer to the following expansions:

$$\boldsymbol{u}^k(\alpha,\beta,z) = \boldsymbol{u}_0^k(\alpha,\beta)+\sin(\frac{\pi z}{h})\boldsymbol{u}_1^k(\alpha,\beta)+\cos(\frac{\pi z}{h})\boldsymbol{u}_2^k(\alpha,\beta)+\sin(\frac{2\pi z}{h})\boldsymbol{u}_3^k(\alpha,\beta)+\cos(\frac{2\pi z}{h})\boldsymbol{u}_4^k(\alpha,\beta) \quad (56)$$

$$\boldsymbol{u}^k(\alpha,\beta,z) = \boldsymbol{u}_0^k(\alpha,\beta) + z\boldsymbol{u}_1^k(\alpha,\beta) + e^{\frac{z}{h}}\boldsymbol{u}_2^k(\alpha,\beta) + e^{\frac{2z}{h}}\boldsymbol{u}_3^k(\alpha,\beta) + (-1)^k\zeta_k\boldsymbol{u}_{4_Z}^k \quad (57)$$

The subscript a denotes the adoption of assumed linear temperature or moisture concentration profiles, whereas c indicates that through-the-thickness distributions are calculated by via Fourier or Fick laws. LW models are indicated as follows:

- "SaSn" indicates a Sampling Surfaces model with n interpolation points.
- "LGDn" indicates a model adopting Legendre polynomials up to the n^{th} order.

Analytical solutions were used in some cases and obtained via the Navier method. In the following tables, N_{exp} is indicated and represents the expansion terms of the model.

Cylindrical cross-ply composite shells under thermal load

In this section, laminated cylindrical shells with layup sequence (0°/90°) (from bottom to top) are analysed. The dimensions are: $a = b = 0.1\text{m}$, $R_\alpha = 0.1\text{m}$, $R_\beta = \infty$, $R_\alpha/h = 2, 10$ and 500. The mechanical properties of the lamina are given in Table 2, and thermal properties in Table 3. The thermal expansion coefficients in the three directions are denoted by α_{11}, α_{22} and α_{33}. The mechanical properties and thermal expansion coefficients are assumed as in [27]. The thermal conduction coefficients K_{11},K_{22} and K_{33} were retrieved from [61]. The thermal load can be described as:

$$\theta(\alpha,\beta,z) = \theta_A(z)\cdot\sin(\frac{m\pi\alpha}{a})\sin(\frac{n\pi\beta}{b}) \quad (58)$$

where the half wave numbers are $m = n = 1$. The temperature boundary conditions are $\theta_A(-\frac{h}{2}) = 0$K and $\theta_A(\frac{h}{2}) = 50$K on the top surface for all cases.

First, a mesh convergence study was carried out, $R_\alpha/h = 500$, subjected to an assumed linear temperature profile. SaS5 was used. Table 4 shows the results. It can be concluded that a mesh of 10×10 is sufficient to ensure the convergence of the FEM solution. The results also show that the adopted MITC9 shell element is locking free and can achieve good accuracies for transverse displacement, normal and shear stresses.

The calculated profiles of temperature for the cylindrical shells are summarized in Fig. 2. Various LW models and temperature profiles were then investigated, as shown in Table 5. It can be stated that:

- The displacement and stress values are in good agreement with the Naiver analytical solution.
- For thick shells, the temperature variation through the thickness can be very different between assumed linear and calculated profiles. Such differences affect the displacement and stress distributions. For moderately thick and thin shells, differences are less evident. It can be concluded that for thin multilayered shell structures, an assumed linear profile can describe the temperature variation, as also shown in [11, 12, 56].
- Thick shells need five expansion terms in each layer; moderately thick shells need four expansion terms, and thin shells three.

Various ESL models were then considered together with the calculated temperature profile. Results are given in Figs. 3 to 6 and Tables 6 to 7. The results suggest that:

- EExp$n$Z and ESnCnZ perform well for thick shells.
- ETnZ and ET1SnCnZ are reliable for thin and thick shells.
- For thick shells, ET11Z and ET1S5C5Z are the recommended models, whereas, in the other cases, ET9Z and ET1S4C4Z should be used.

Cylindrical cross-ply composite shells under hygroscopic load

The same multilayered structure, loading conditions and mesh of the previous section are here adopted. The material properties can be found in Table 2 and Table 8.

LW models were considered first, and the results are given in Figs. 7 and 8 and Table 9. It can be stated that:

- LW models can provide satisfactory accuracies if compared to the analytical results.
- For moderately thick and thin shells, the linear moisture concentration variation through the thickness is a reasonable assumption.
- Stress distributions present variations quite similar to thermal cases.

Various ESL models are then considered, as shown in Table 10 and Fig. 9. It can be concluded that for shells with aspect ratios $R_\alpha = 2, 10$ and 500, the expansion terms needed are 13, 11, and 9 respectively. These numbers are 9, 7, and 5 for LW models. Therefore, ESL models are not as efficient as LW for these cases.

Conclusions

Various and miscellaneous approximation theories with arbitrary number of expansion terms have been here integrated in the framework of CUF for the analysis of multilayered structures. The steady state mechanical responses of composite cylindrical shells under thermal/hygroscopic loads have been studied with CUF-based variable kinematics adopting LW and ESL approaches, respectively. A MITC9 shell element is employed to guarantee locking free FEM analysis. Both assumed linear temperature/moisture concentration profiles through the thickness, and calculated variations (by solving the diffusion law) are considered. The analogy between heat conduction and moisture diffusion plays a key role when expanding the analysis methodology of thermoelastic problems to hygrothermal ones. Transverse displacement and stresses have been reported for various aspect ratios. The convergence rates of various kinematics have been compared. Based on the above work, some conclusions can be drawn as:

1. For laminates with various aspect ratios, the numbers of expansion terms necessary to obtain converged numerical results are usually different, and thick laminates need more expansion terms.
2. When applied to hygrothermal analysis, classical theories such as FSDT gives incorrect results even for thin laminates.
3. For thin shells, linear variation of temperature/moisture concentration through the thickness is a sufficient assumption, whereas for thick layered shells this assumption can lead to over estimated

stress evaluation compared with results using profiles obtained by solving Fourier heat conduction equation or Fick Law.

4. For the hygrothermal cases studied, LW models employing Legendre polynomials of the fourth-order (LGD4) and the Sampling Surfaces method with five interpolation nodes (SaS5) can guarantee continuous transverse shear stress distribution through the thickness for composite laminates with a broad range of length to thickness ratios (from 2 to 500).

5. Variable ESL kinematics ETnZ and ET1SnCnZ have been tested. It has been demonstrated that when a sufficient number of expansion terms are used, with the help of the Murakami zig-zag function, ETnZ, and ET1SnCnZ are capable of capturing transverse shear stress distribution through the thickness the two-layer shells. In some cases, these two classes of ESL kinematics can be more computationally efficient than LW models with comparable accuracy.

6. Compared with ESL models, LW models can provide results with better accuracy in approximating the through the thickness distribution of transverse shear stresses in composite laminates.

A companion work to this one is devoted to the modelling of composite plates with symmetric lamination subjected to hygrothermal loads. In that paper, very similar conclusions about the accuracy of the models used are drawn.
Future works should be devoted to the axiomatic/asymptotic analysis of the influence of each term and the definition of Best Theory Diagrams, as in [62].

Acknowledgment

This research work has been carried out within the project FULLCOMP (FULLy analysis, design, manufacturing, and health monitoring of COMPosite structures), funded by the European Union Horizon 2020 Research and Innovation program under the Marie Skłodowska Curie grant agreement No. 642121. E. Carrera has been partially supported by the Russian Science Foundation (Grant No. 15-19-30002).

References

[1] R. B. Pipes, J. R. Vinson, and T. W. Chou, "On the hygrothermal response of laminated composite systems," *Journal of Composite Materials*, vol. 10, no. 2, pp. 129–148, 1976.

[2] G. C. Sih, J. Michopoulos, and S. C. Chou, *Hygrothermoelasticity*. Springer Science & Business Media, Dec. 2012.

[3] C. J. Miller, T. Kicher, and W. Millavec, "Thermal stress analysis of layered cylindrical shells," *AIAA Journal*, vol. 19, no. 4, pp. 523–530, 1981.

[4] P. Dumir, J. Nath, P. Kumari, and S. Kapuria, "Improved efficient zigzag and third order theories for circular cylindrical shells under thermal loading," *Journal of Thermal Stresses*, vol. 31, no. 4, pp. 343–367, 2008.

[5] Z. Wu and W. Chen, "A global-local higher order theory for multilayered shells and the analysis of laminated cylindrical shell panels," *Composite Structures*, vol. 84, no. 4, pp. 350–361, 2008.

[6] R. K. Khare, T. Kant, and A. K. Garg, "Closed-form thermo-mechanical solutions of higher-order theories of cross-ply laminated shallow shells," *Composite Structures*, vol. 59, no. 3, pp. 313–340, 2003.

[7] A. Khdeir, "Thermoelastic analysis of cross-ply laminated circular cylindrical shells," *International Journal of Solids and Structures*, vol. 33, no. 27, pp. 4007–4017, 1996.

[8] A. A. Khdeir, M. D. Rajab, and J. N. Reddy, "Thermal effects on the response of cross-ply laminated shallow shells," *International Journal of Solids and Structures*, vol. 29, no. 5, pp. 653–667, 1992.

[9] A. Barut, E. Madenci, and A. Tessler, "Nonlinear thermoelastic analysis of composite panels under non-uniform temperature distribution," *International Journal of Solids and Structures*, vol. 37, no. 27, pp. 3681–3713, 2000.

[10] V. Tungikar and K. M. Rao, "Three dimensional exact solution of thermal stresses in rectangular composite laminate," *Composite Structures*, vol. 27, no. 4, pp. 419–430, 1994.

[11] E. Carrera, "Temperature profile influence on layered plates response considering classical and advanced theories," *AIAA Journal*, vol. 40, no. 9, pp. 1885–1896, 2002.

[12] M. Cinefra, S. Valvano, and E. Carrera, "Heat conduction and thermal stress analysis of laminated composites by a variable kinematic MITC9 shell element," *Curved and Layered Structures*, vol. 2, no. 1, pp. 301–320, 2015.

[13] J. Fourier, *Theorie analytique de la chaleur, par M. Fourier.* Chez Firmin Didot, père et fils, 1822.

[14] A. Fick, "On liquid diffusion," *Journal of Membrane Science*, vol. 100, no. 1, pp. 33–38, 1995.

[15] C. H. Shen and G. S. Springer, "Moisture absorption and desorption of composite materials," *Journal of Composite Materials*, vol. 10, no. 1, pp. 2–20, 1976.

[16] S. W. Tsai and T. N. Massard, *Composites design.* Think Composites, 1988.

[17] A. Szekeres and J. Engelbrecht, "Coupled thermal and moisture fields with application to composites," *Periodica Polytechnica. Engineering. Mechanical Engineering*, vol. 41, no. 2, p. 151, 1997.

[18] A. Szekeres, "Analogy between heat and moisture: Thermo-hygro-mechanical tailoring of composites by taking into account the second sound phenomenon," *Computers & Structures*, vol. 76, no. 1, pp. 145–152, 2000.

[19] A. Benkeddad, M. Grediac, and A. Vautrin, "On the transient hygroscopic stresses in laminated composite plates," *Composite Structures*, vol. 30, no. 2, pp. 201–215, 1995.

[20] A. Benkeddad, M. Grediac, and A. Vautrin, "Computation of transient hygroscopic stresses in laminated composite plates," *Composites Science and Technology*, vol. 56, no. 7, pp. 869–876, 1996.

[21] A. Tounsi, M. Bouazza, and E. A. Bedia, "Computation of transient hygroscopic stresses in unidirectional laminated composite plates with cyclic and asymmetrical environmental conditions," *International Journal of Mechanics and Materials in Design*, vol. 1, no. 3, pp. 271–286, 2004.

[22] A. Tounsi and E. A. Bedia, "Simplified method for prediction of transient hygroscopic stresses in polymer matrix composites with symmetric environmental conditions," *Applied Composite Materials*, vol. 10, no. 1, pp. 1–18, 2003.

[23] A. Tounsi and E. A. Bedia, "Some observations on the evolution of transversal hygroscopic stresses in laminated composites plates: effect of anisotropy," *Composite Structures*, vol. 59, no. 4, pp. 445–454, 2003.

[24] A. Tounsi, E. A. Bedia, and A. Benachour, "A new computational method for prediction of transient hygroscopic stresses during moisture desorption in laminated composite plates with different degrees of anisotropy," *Journal of Thermoplastic Composite Materials*, vol. 18, no. 1, pp. 37–58, 2005.

[25] E. A. Bedia, W. Han, and G. Verchery, "An asymptotic characterisation of the moisture diffusion in polymer matrix composites with cyclic environmental conditions," *Composite Structures*, vol. 49, no. 3, pp. 269–274, 2000.

[26] B. Boukhoulda, E. A. Bedia, and K. Madani, "The effect of fiber orientation angle in composite materials on moisture absorption and material degradation after hygrothermal ageing," *Composite Structures*, vol. 74, no. 4, pp. 406–418, 2006.

[27] F. Jacquemin and A. Vautrin, "A closed-form solution for the internal stresses in thick composite cylinders induced by cyclical environmental conditions," *Composite Structures*, vol. 58, no. 1, pp. 1–9, 2002.

[28] B. Patel, M. Ganapathi, and D. Makhecha, "Hygrothermal effects on the structural behaviour of thick composite laminates using higher-order theory," *Composite Structures*, vol. 56, no. 1, pp. 25–34, 2002.

[29] S. Lo, W. Zhen, Y. Cheung, and C. Wanji, "Hygrothermal effects on multilayered composite plates using a refined higher order theory," *Composite Structures*, vol. 92, no. 3, pp. 633–646, 2010.

[30] S. Alsubari, J. M. Ali, and Y. Aminanda, "Hygrothermoelastic analysis of anisotropic cylindrical shells," *Composite Structures*, vol. 131, pp. 151–159, 2015.

[31] E. Carrera, "Theories and finite elements for multilayered, anisotropic, composite plates and shells," *Archives of Computational Methods in Engineering*, vol. 9, no. 2, pp. 87–140, 2002.

[32] E. Carrera, "Theories and finite elements for multilayered plates and shells: a unified compact formulation with numerical assessment and benchmarking," *Archives of Computational Methods in Engineering*, vol. 10, no. 3, pp. 215–296, 2003.

[33] E. Carrera, M. Cinefra, and F. A. Fazzolari, "Some results on thermal stress of layered plates and shells by using Unified Formulation," *Journal of Thermal Stresses*, vol. 36, no. 6, pp. 589–625, 2013.

[34] M. Cinefra, E. Carrera, S. Brischetto, and S. Belouettar, "Thermo-mechanical analysis of functionally graded shells," *Journal of Thermal Stresses*, vol. 33, no. 10, pp. 942–963, 2010.

[35] M. Cinefra, S. Valvano, and E. Carrera, "Thermal stress analysis of laminated structures by a variable kinematic MITC9 shell element," *Journal of Thermal Stresses*, vol. 39, no. 2, pp. 121–141, 2016.

[36] E. Carrera, F. Fazzolari, and M. Cinefra, *Thermal Stress Analysis of Composite Beams, Plates and Shells*. Elsevier, 2015.

[37] K. J. Bathe, P. S. Lee, and J. F. Hiller, "Towards improving the MITC9 shell element," *Computers & Structures*, vol. 81, no. 8, pp. 477–489, 2003.

[38] C. Chinosi and L. Della Croce, "Mixed-interpolated elements for thin shells," *Communications in Numerical Methods in Engineering*, vol. 14, no. 12, pp. 1155–1170, 1998.

[39] H. C. Huang, "Membrane locking and assumed strain shell elements," *Computers & Structures*, vol. 27, no. 5, pp. 671–677, 1987.

[40] P. Panasz and K. Wisniewski, "Nine-node shell elements with 6 dofs/node based on two-level approximations. part i: Theory and linear tests," *Finite Elements in Analysis and Design*, vol. 44, no. 12, pp. 784–796, 2008.

[41] E. Carrera, M. Cinefra, G. Li, and G. Kulikov, "MITC9 shell finite elements with miscellaneous through-the-thickness functions for the analysis of laminated structures," *Composite Structures*, vol. 154, pp. 360–373, 2016.

[42] A. W. Leissa, "Vibration of Shells," tech. rep., Jan. 1973.

[43] R. M. Jones, *Buckling of bars, plates, and shells*. Bull Ridge Corporation, 2006.

[44] J. Reddy, *Mechanics of laminated composite plates and shells. Theory and Analysis*. CRC Press, 2^{nd} ed., 2004.

[45] P. M. Naghdi, "The theory of plates and shells," *Handbuch der Physik, vol. VI a/2*, pp. 425–640, 1972.

[46] W. Koiter, "On the foundations of the linear theory of thin elastic shell," *Proc Kon Nederl Akad Wetensch*, vol. 73, no. 3, pp. 169–195, 1970.

[47] P. G. Ciarlet and L. Gratie, "Another approach to linear shell theory and a new proof of korn's inequality on a surface," *Comptes Rendus Mathematique*, vol. 340, no. 6, pp. 471–478, 2005.

[48] H. Murakami, "Laminated composite plate theory with improved in-plane responses," *Journal of Applied Mechanics*, vol. 53, no. 3, pp. 661–666, 1986.

[49] I. Babuska, B. A. Szabo, and I. N. Katz, "The p-version of the finite element method," *SIAM Journal on Numerical Analysis*, vol. 18, no. 3, pp. 515–545, 1981.

[50] A. Pagani, A. de Miguel, M. Petrolo, and E. Carrera, "Analysis of laminated beams via Unified Formulation and Legendre polynomial expansions," *Composite Structures*, vol. 156, pp. 78 – 92, 2016.

[51] L. Demasi, "Mixed plate theories based on the Generalized Unified Formulation.: Part ii: Layerwise theories," *Composite Structures*, vol. 87, no. 1, pp. 12 – 22, 2009.

[52] E. Carrera and G. Giunta, "Hierarchical evaluation of failure parameters in composite plates," *AIAA Journal*, vol. 47, no. 3, pp. 692–702, 2009.

[53] G. Kulikov and S. Plotnikova, "Exact 3D stress analysis of laminated composite plates by sampling surfaces method," *Composite Structures*, vol. 94, no. 12, pp. 3654–3663, 2012.

[54] G. Kulikov and S. Plotnikova, "Advanced formulation for laminated composite shells: 3D stress analysis and rigid-body motions," *Composite Structures*, vol. 95, pp. 236–246, 2013.

[55] G. Kulikov and S. Plotnikova, "Hybrid-mixed ans finite elements for stress analysis of laminated composite structures: Sampling surfaces plate formulation," *Computer Methods in Applied Mechanics and Engineering*, vol. 303, pp. 374–399, 2016.

[56] M. Cinefra and S. Valvano, "A variable kinematic doubly-curved MITC9 shell element for the analysis of laminated composites," *Mechanics of Advanced Materials and Structures*, vol. 23, no. 11, pp. 1312–1325, 2016.

[57] M. Cinefra, E. Carrera, L. Della Croce, and C. Chinosi, "Refined shell elements for the analysis of functionally graded structures," *Composite Structures*, vol. 94, pp. 415–422, 2012.

[58] M. Cinefra, C. Chinosi, and L. Della Croce, "Mitc9 shell elements based on refined theories for the analysis of isotropic cylindrical structures," *Mechanics of Advanced Materials and Structures*, vol. 20, pp. 91–100, 2013.

[59] M. Cinefra and E. Carrera, "Shell finite elements with different through-the-thickness kinematics for the linear analysis of cylindrical multilayered structures," *International Journal for Numerical Methods in Engineering*, vol. 93, pp. 160–182, 2013.

[60] M. Cinefra, "Free-vibration analysis of laminated shells via refined mitc9 elements," *Mechanics of Advanced Materials and Structures*, vol. 23, no. 9, pp. 937–947, 2016.

[61] M. T. Hicks, "Design of a carbon fiber composite grid structure for the glast spacecraft using a novel manufacturing technique," tech. rep., SLAC, 2001.

[62] E. Carrera, M. Cinefra, M. Petrolo, and A. Lamberti, "Best theory diagrams for multilayered plates considering multifield analysis," *Journal of Intelligent Material Systems and Structures*, vol. In Press.

Table 1: Expansion terms of the ESL models.

	z^0	$z^1 \to z^N$	$(-1)^k\zeta_k$	$\sin\left(\frac{z\pi}{h}\right) \to \sin\left(\frac{nz\pi}{h}\right)$	$\cos\left(\frac{z\pi}{h}\right) \to \cos\left(\frac{nz\pi}{h}\right)$	$e^{(z/h)} \to e^{(nz/h)}$
ETn	√	√	×	×	×	×
ETnZ	√	√	√	×	×	×
ESn	√	×	×	√	×	×
ESnZ	√	×	√	√	×	×
ECn	√	×	×	×	√	×
ECnZ	√	×	√	×	√	×
ESnCn	√	×	×	√	√	×
ESnCnZ	√	×	√	√	√	×
ETnSnCn	√	√	×	√	√	×
ETnSnCnZ	√	√	√	√	√	×
EEXPn	√	×	×	×	×	√
EEXPnZ	√	×	√	×	×	√
ETnEXPn	√	√	×	×	×	√
ETnEXPnZ	√	√	√	×	×	√

Table 2: Mechanical properties of T300/5208 composite lamina

E_1(GPa)	E_2, E_3(GPa)	G_{12}, G_{13}(GPa)	G_{23}(GPa)	ν_{12}, ν_{13}	ν_{23}
181	10.3	7.17	2.39	0.28	0.43

Table 3: Thermal properties of T300/5208 composite lamina [16]

α_{11} (10^{-6}/K)	α_{22}, α_{33} (10^{-6}/K)	K_{11} (W/mK)	K_{22}, K_{33} (W/mK)
0.02	22.5	4.6	0.7

Table 4: Convergence study, with LW kinematics SaS5, assumed linear temperature profiles are adopted. Displacement and stress evaluation for bending analysis for two-layer composite cylindrical shells with $R_\alpha/h = 500$ subjected to thermal load.

$R_\alpha/_h$	Mesh	$^{\S}w$ 10^{-3}mm	$^{\dagger}\sigma_{\alpha\alpha}$ KPa	$^{\ddagger}\sigma_{\alpha z}$ KPa
500	4×4	8.228	-11014	15.10
	6×6	8.226	-11021	15.12
	8×8	8.225	-11023	15.11
	10×10	8.225	-11024	15.10
	*LGD4$_a$	8.2246	-11025	15.070

Variables are evaluated at: $^{\S}(\frac{a}{2}, \frac{b}{2}, \frac{h}{2})$; $^{\dagger}(\frac{a}{2}, \frac{b}{2}, \frac{h}{2})$; $^{\ddagger}(a, \frac{b}{2}, \frac{h}{4})$.

* Navier-type analytical solution.

Table 5: Displacement and stress evaluation for bending analysis for two-layer composite cylindrical shells with various R_α/h value subjected to thermal load, obtained with LW models. Linear and calculated profiles are used.

R_α/h	Model	Assumed profiles			Calculated profiles			N_{exp}
		$^{\S}w$	$^{\dagger}\sigma_{\alpha\alpha}$	$^{\ddagger}\sigma_{\alpha z}$	$^{\S}w$	$^{\dagger}\sigma_{\alpha\alpha}$	$^{\ddagger}\sigma_{\alpha z}$	
		10^{-3}mm	KPa	KPa	10^{-3}mm	KPa	KPa	
2	SaS4	27.39	-4181.6	264.0	16.39	-7272	536.7	7
	SaS5	27.39	-4271.0	261.1	16.39	-7074	538.3	9
	SaS6	27.39	-4286.3	265.9	16.40	-7045	537.2	11
	LGD1	25.28	-6097	595.8	14.78	-11474	579.4	3
	LGD4	27.39	-4271	261.1	16.39	-7074	538.3	9
	⋆LGD4	27.393	-4287.8	260.56	16.403	-7073.4	541.76	9
10	SaS4	19.11	-8847	554.4	18.57	-8957	544.6	7
	SaS5	19.11	-8849	554.4	18.57	-8952	544.6	9
	LGD1	20.51	-10607	587.2	19.98	-11003	577.5	3
	LGD4	19.11	-8849	554.4	18.57	-8952	544.6	9
	⋆LGD4	19.110	-8854.6	553.23	18.570	-8957.6	543.49	9
500	SaS4	8.225	-11024	15.10	8.225	-11024	15.10	7
	SaS5	8.225	-11024	15.10	8.225	-11024	15.10	9
	LGD1	8.325	-13271	15.53	8.325	-13271	15.53	3
	LGD4	8.225	-11024	15.10	8.225	-11024	15.10	9
	⋆LGD4	8.2246	-11025	15.070	8.2244	-11025	15.069	9

Variables are evaluated at: $^{\S}(\frac{a}{2}, \frac{b}{2}, \frac{h}{2})$; $^{\dagger}(\frac{a}{2}, \frac{b}{2}, \frac{h}{2})$; $^{\ddagger}(a, \frac{b}{2}, \frac{h}{4})$.

* Navier-type analytical solution.

Table 6: Displacement and stress evaluation of two-layer composite cylindrical shells with various R_α/h subjected to thermal load, obtained with ESL models EExp$n$Z and ESnCnZ. Calculated temperature profiles are used.

$R_\alpha/_h$	Model	$^{\S}w$ 10^{-3}mm	$^{\dagger}\sigma_{\alpha\alpha}$ KPa	$^{\ddagger}\sigma_{\alpha z}$ KPa	N_{exp}
2	FSDT$_c$	5.239	-14985	162.8	2*
	EExp5Z$_c$	16.38	-6999	586.4	7
	EExp7Z$_c$	16.39	-7064	531.8	9
	EExp9Z$_c$	16.39	-7043	506.6	11
	ES3C3Z$_c$	16.37	-7485	525.1	8
	ES4C4Z$_c$	16.39	-7167	503.3	10
	ES5C5Z$_c$	16.40	-7059	507.6	12
	*LGD4$_c$	16.403	-7073.4	541.76	9
10	FSDT$_c$	22.79	-14890	350.9	2*
	EExp5Z$_c$	18.55	-8967	604.0	7
	EExp7Z$_c$	18.56	-8963	545.4	9
	EExp9Z$_c$	18.57	-8906	460.2	11
	ES3C3Z$_c$	18.53	-9324	523.7	8
	ES4C4Z$_c$	18.56	-9044	524.5	10
	ES5C5Z$_c$	18.57	-8964	531.9	12
	*LGD4$_c$	18.570	-8957.6	543.49	9
500	FSDT$_c$	14.47	-16891	10.67	2*
	EExp5Z$_c$	8.224	-11080	17.02	7
	EExp7Z$_c$	8.225	-11028	15.13	9
	EExp9Z$_c$	8.224	-10878	17.77	11
	ES3C3Z$_c$	8.184	-11415	1.951	8
	ES4C4Z$_c$	8.223	-11110	13.18	10
	ES5C5Z$_c$	8.224	-11042	15.68	12
	*LGD4$_c$	8.2244	-11025	15.069	9

Variables are evaluated at: $^{\S}(\frac{a}{2}, \frac{b}{2}, \frac{h}{2})$; $^{\dagger}(\frac{a}{2}, \frac{b}{2}, \frac{h}{2})$; $^{\ddagger}(a, \frac{b}{2}, \frac{h}{4})$.

* Navier-type analytical solution.

Table 7: Displacement and stress evaluation of two-layer composite cylindrical shells with various R_α/h subjected to thermal load, obtained with ESL models ETnZ and ET1SnCnZ. Calculated temperature profiles are applied.

$R_\alpha/_h$	Model	$^{\S}w$ 10^{-3}mm	$^{\dagger}\sigma_{\alpha\alpha}$ KPa	$^{\ddagger}\sigma_{\alpha z}$ KPa	N_{exp}
2	FSDT$_c$	5.239	-14985	162.8	2*
	ET7Z$_c$	16.39	-7072	527.5	9
	ET9Z$_c$	16.39	-7026	511.4	11
	ET11Z$_c$	16.40	-7081	513.1	13
	ET1S3C3Z$_c$	16.39	-7124	522.9	9
	ET1S4C4Z$_c$	16.39	-7040	509.1	11
	ET1S5C5Z$_c$	16.40	-7057	516.2	13
	*LGD4$_c$	16.403	-7073.4	541.76	9
10	FSDT$_c$	22.79	-14890	350.9	2*
	ET5Z$_c$	18.56	-8936	567.2	7
	ET7Z$_c$	18.56	-8963	543.2	9
	ET9Z$_c$	18.57	-8944	532.3	11
	ET1S2C2Z$_c$	18.57	-9064	561.4	7
	ET1S3C3Z$_c$	18.57	-8983	538.9	9
	ET1S4C4Z$_c$	18.57	-8949	531.5	11
	*LGD4$_c$	18.570	-8957.6	543.49	9
500	FSDT$_c$	14.47	-16891	10.67	2*
	ET3Z$_c$	8.225	-11024	15.66	5
	ET5Z$_c$	8.225	-11024	15.66	7
	ET7Z$_c$	8.225	-11024	15.13	9
	ET1S1C1Z$_c$	8.229	-11772	15.51	5
	ET1S2C2Z$_c$	8.225	-11154	15.43	7
	ET1S3C3Z$_c$	8.225	-11047	15.06	9
	*LGD4$_c$	8.2244	-11025	15.069	9

Variables are evaluated at: $^{\S}(\frac{a}{2}, \frac{b}{2}, \frac{h}{2})$; $^{\dagger}(\frac{a}{2}, \frac{b}{2}, \frac{h}{2})$; $^{\ddagger}(a, \frac{b}{2}, \frac{h}{4})$.

* Navier-type analytical solution.

Table 8: Hygroscopic properties of T300/5208 composite lamina [16]

β_{11} $(\text{wt.\%H}_2\text{O})^{-1}$	β_{22}, β_{33} $(\text{wt.\%H}_2\text{O})^{-1}$	D_{11} (mm^2/s)	D_{22}, D_{33} (mm^2/s)
0	0.006	2.87×10^{-8}	1.63×10^{-8}

Table 9: Displacements and stresses of the composite cylindrical shells with various R_α/h under hygroscopic load, obtained with LW models. Linear and calculated moisture concentration profiles are used.

$R_\alpha/_h$	Model	Assumed profiles			Calculated profiles			N_{exp}
		$^{\S}w$ 10^{-3}mm	$^{\dagger}\sigma_{\alpha\alpha}$ MPa	$^{\ddagger}\sigma_{\alpha z}$ MPa	$^{\S}w$ 10^{-3}mm	$^{\dagger}\sigma_{\alpha\alpha}$ MPa	$^{\ddagger}\sigma_{\alpha z}$ MPa	
2	SaS4	146.0	-22.30	1.417	113.9	-30.74	2.418	7
	SaS5	146.0	-22.78	1.402	113.9	-30.76	2.411	9
	LGD1	134.8	-32.51	3.189	104.1	-47.83	3.254	3
	LGD4	146.0	-22.78	1.402	113.9	-30.76	2.411	9
	*LGD4	146.01	-22.869	1.3991	113.21	-31.009	2.4303	9
10	SaS4	101.5	-47.22	2.961	100.5	-47.43	2.942	7
	SaS5	101.5	-47.23	2.961	100.5	-47.43	2.942	9
	LGD1	109.0	-56.60	3.136	108.0	-57.39	3.117	3
	LGD4	101.5	-47.23	2.961	100.5	-47.43	2.942	9
	*LGD4	101.53	-47.258	2.9547	100.46	-47.461	2.9355	9
500	SaS4	43.36	-58.80	0.08053	43.36	-58.80	0.08053	7
	SaS5	43.36	-58.80	0.08053	43.36	-58.80	0.08053	9
	LGD1	43.90	-70.79	0.08282	43.90	-70.79	0.08282	3
	LGD4	43.36	-58.80	0.08053	43.36	-58.80	0.08053	9
	*LGD4	43.359	-58.808	0.080387	43.359	-58.808	0.080387	9

Variables are evaluated at: $^{\S}(\frac{a}{2}, \frac{b}{2}, \frac{h}{2})$; $^{\dagger}(\frac{a}{2}, \frac{b}{2}, \frac{h}{2})$; $^{\ddagger}(a, \frac{b}{2}, \frac{h}{4})$.

* Navier-type analytical solution.

Table 10: Displacement and stress evaluation for the composite cylindrical shells with various R_α/h subjected to hygroscopic load, obtained with ESL models ETnZ and ET1SnCnZ. Calculated moisture profiles are used.

$R_\alpha/_h$	Model	$^{\S}w$ 10^{-3}mm	$^{\dagger}\sigma_{\alpha\alpha}$ MPa	$^{\ddagger}\sigma_{\alpha z}$ MPa	N_{exp}
2	FSDT$_c$	34.14	-75.38	1.215	2*
	ET7Z$_c$	113.9	-31.03	2.347	9
	ET9Z$_c$	113.9	-30.67	2.198	11
	ET11Z$_c$	113.9	-30.96	2.214	13
	ET1S3C3Z$_c$	113.9	-31.12	2.273	9
	ET1S4C4Z$_c$	113.9	-30.72	2.183	11
	ET1S5C5Z$_c$	113.9	-30.94	2.251	13
	*LGD4$_c$	113.21	-31.009	2.4303	9
10	FSDT$_c$	123.1	-79.09	1.921	2*
	ET5Z$_c$	100.4	-47.34	3.068	7
	ET7Z$_c$	100.4	-47.49	2.934	9
	ET9Z$_c$	100.5	-47.39	2.874	11
	ET1S2C2Z$_c$	100.4	-47.99	3.036	7
	ET1S3C3Z$_c$	100.4	-47.59	2.910	9
	ET1S4C4Z$_c$	100.5	-47.42	2.869	11
	*LGD4$_c$	100.46	-47.461	2.9355	9
500	FSDT$_c$	76.64	-90.10	0.05690	2*
	ET3Z$_c$	43.36	-58.80	0.08356	5
	ET5Z$_c$	43.36	-58.80	0.08286	7
	ET7Z$_c$	43.36	-58.80	0.08071	9
	ET1S1C1Z$_c$	43.38	-62.79	0.08274	5
	ET1S2C2Z$_c$	43.36	-59.50	0.08233	7
	ET1S3C3Z$_c$	43.36	-58.93	0.08036	9
	*LGD4$_c$	43.359	-58.808	0.080387	9

Variables are evaluated at: $^{\S}(\frac{a}{2}, \frac{b}{2}, \frac{h}{2})$; $^{\dagger}(\frac{a}{2}, \frac{b}{2}, \frac{h}{2})$; $^{\ddagger}(a, \frac{b}{2}, \frac{h}{4})$.

* Navier-type analytical solution.

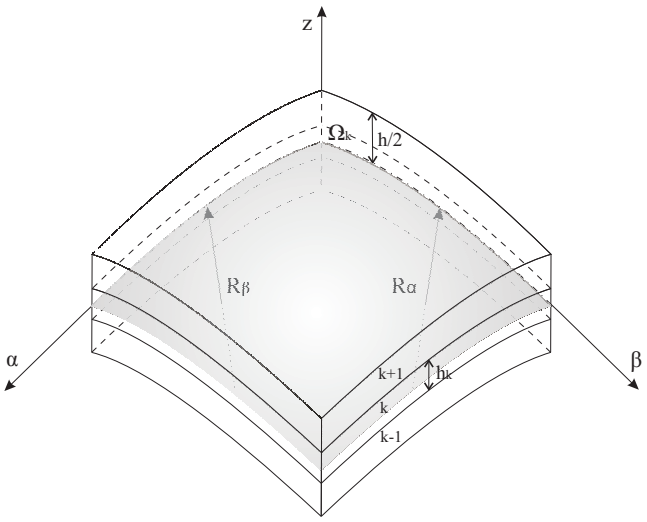

Figure 1: Multilayered doubly curved shell: notation and geometry.

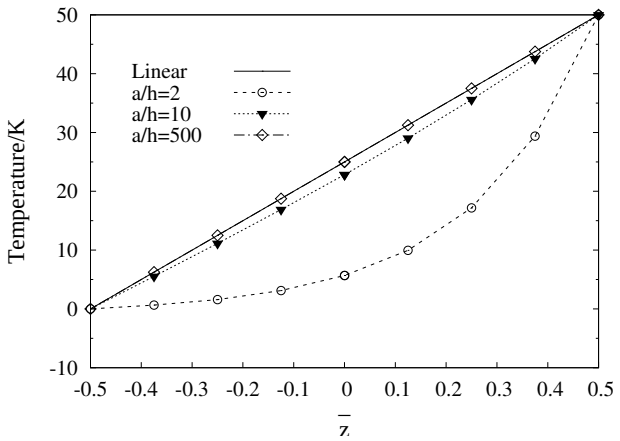

Figure 2: Temperature profiles $\theta_A(z)$ for composite cylindrical shells of various thickness ratios (R_α/h) subjected to thermal load.

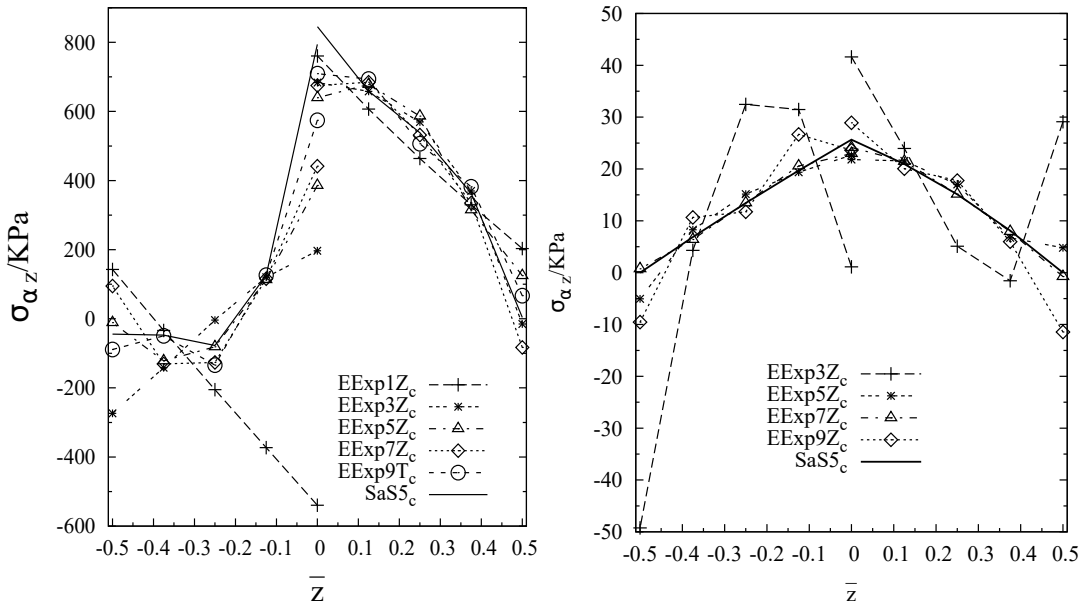

(a) $R_\alpha/h = 2$ (b) $R_\alpha/h = 500$

Figure 3: Transverse shear stress $\sigma_{\alpha z}$ through the thickness of the composite shells with various R_α/h ratios, obtained by ESL models adopting EExp$n$Z, with calculated temperature profiles.

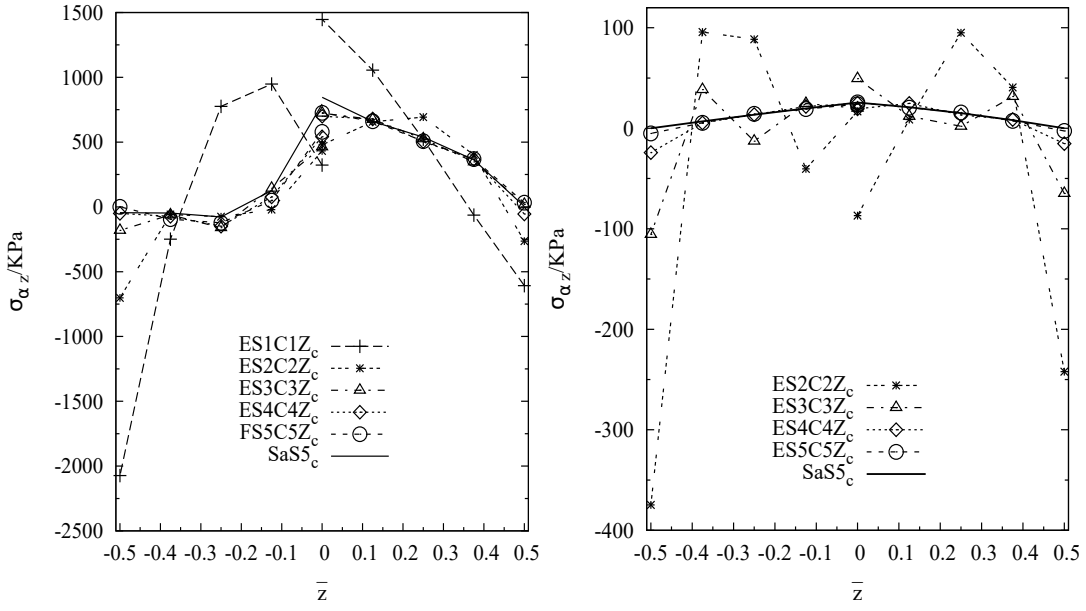

(a) $R_\alpha/h = 2$ (b) $R_\alpha/h = 500$

Figure 4: Transverse shear stress $\sigma_{\alpha z}$ through the thickness of the composite shells with various R_α/h ratios subjected to thermal load, obtained by ESL models adopting ESnCnZ, calculated temperature profiles are used.

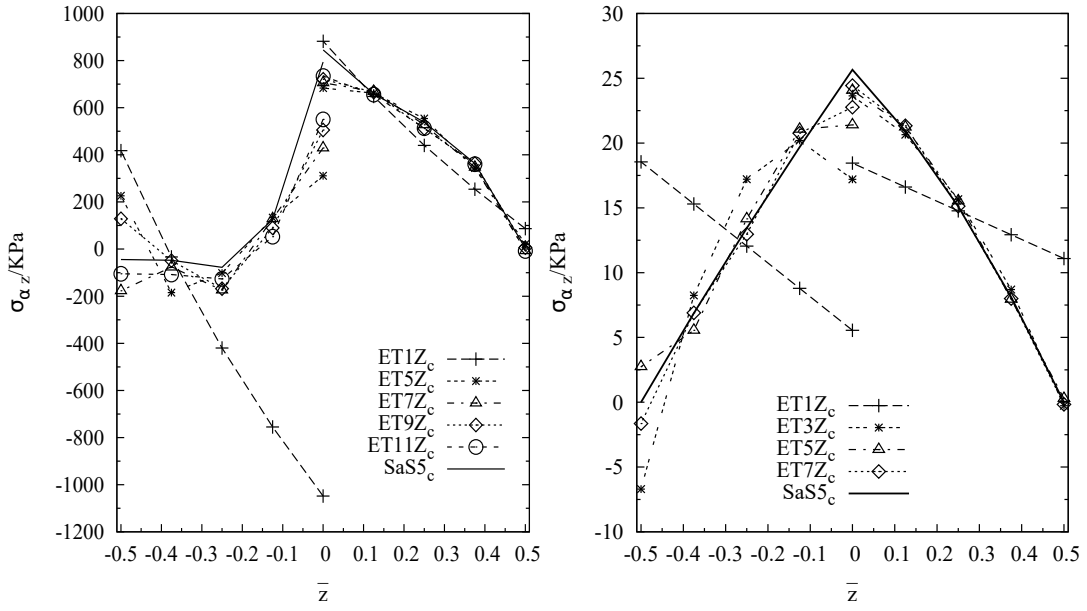

(a) $R_\alpha/h = 2$ (b) $R_\alpha/h = 500$

Figure 5: Transverse shear stress $\sigma_{\alpha z}$ through the thickness of the composite shells with various R_α/h ratios subjected to thermal load, obtained by ESL models adopting ETnZ, calculated temperature profiles are used.

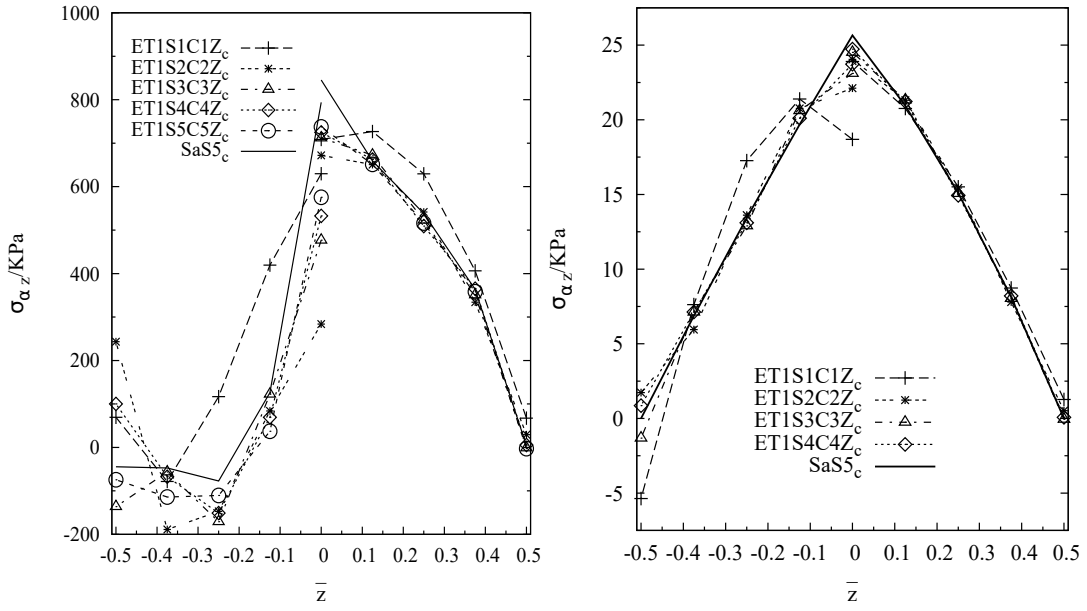

(a) $R_\alpha/h = 2$ (b) $R_\alpha/h = 500$

Figure 6: Transverse shear stress $\sigma_{\alpha z}$ through the thickness of the composite shells with various R_α/h ratios subjected to thermal load, obtained by ESL models adopting ET1SnCnZ, calculated temperature profiles are used.

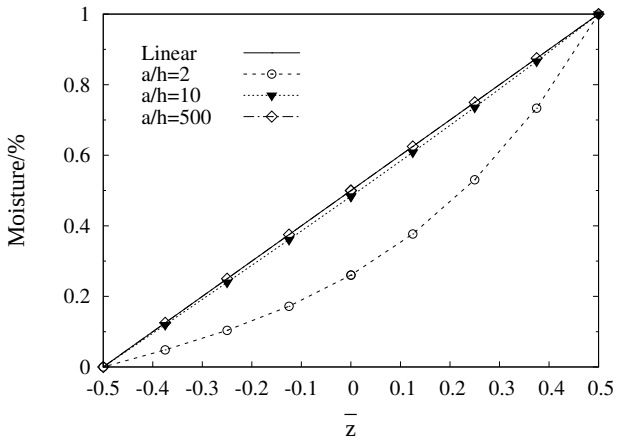

Figure 7: Moisture concentration profiles of composite shells with various R_α/h under hygroscopic load.

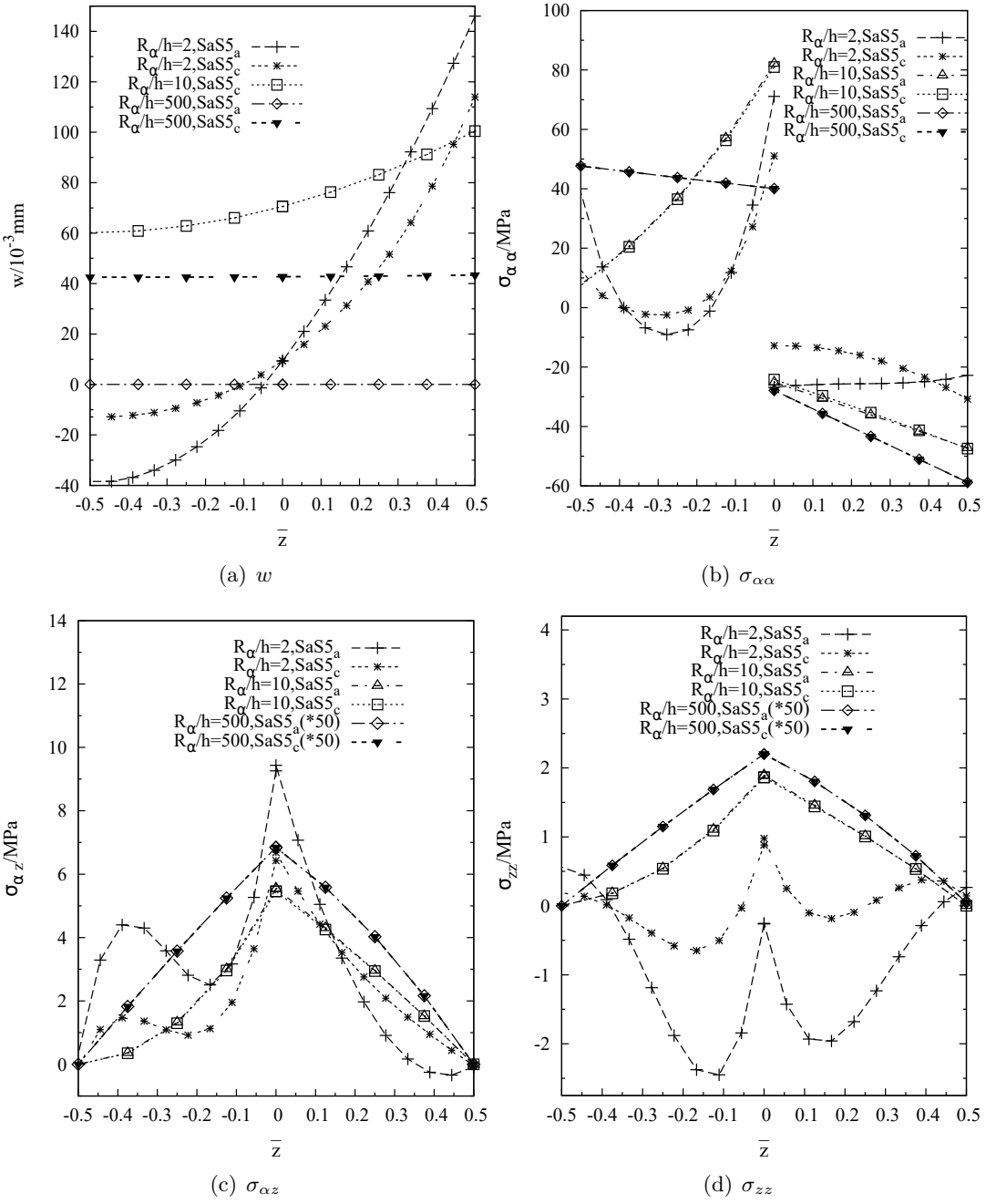

(a) w (b) $\sigma_{\alpha\alpha}$

(c) $\sigma_{\alpha z}$ (d) σ_{zz}

Figure 8: Transverse displacement w and stresses through the thickness of the composite cylindrical shells with various R_α/h ratios under hygroscopic load, SaS5 solutions with both linear and calculated profiles.

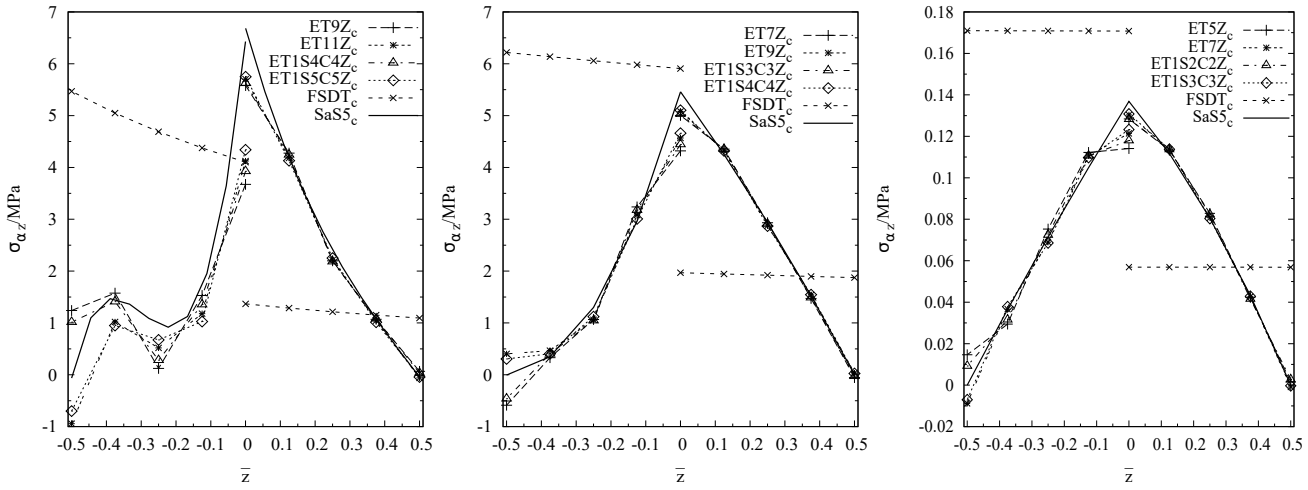

(a) $R_\alpha/h = 2$ (b) $R_\alpha/h = 10$ (c) $R_\alpha/h = 500$

Figure 9: Transverse shear stress $\sigma_{\alpha z}$ through the thickness of the composite shells with various R_α/h ratios under hygroscopic load, obtained by models with various thickness functions. Assumed linear and calculated profiles are used.